

# Fluctuations and Correlations of Conserved Charges near the QCD Critical Point

Wei-jie Fu<sup>1,\*</sup> and Yue-liang Wu<sup>1,†</sup>

<sup>1</sup>*Kavli Institute for Theoretical Physics China (KITPC),*

*Key Laboratory of Frontiers in Theoretical Physics, Institute of Theoretical Physics,  
Chinese Academy of Science, Beijing 100190, China*

(Dated: February 22, 2019)

## Abstract

We study the fluctuations and correlations of conserved charges, i.e. the baryon number, electric charge and the strangeness at finite temperature and nonzero baryon chemical potential with an effective model. The fluctuations are calculated up to the fourth-order and the correlations to the third-order. We find that the second-order fluctuations and correlations have a peak or valley structure when the chiral phase transition takes place with the increase of the baryon chemical potential; the third-order fluctuations and correlations change their signs during the chiral phase transition and the fourth-order fluctuations have two maximum and one minimum. we also depict contour plots of various fluctuations and correlations of conserved charges in the plane of temperature and baryon chemical potential. We find that higher order fluctuations and correlations of conserved charges are superior to the second-order ones to be used to search for the critical point in heavy ion collision experiments.

PACS numbers: 12.38.Mh, 24.60.Ky, 11.30.Rd, 25.75.Nq

---

\*wjfu@itp.ac.cn

†ylwu@itp.ac.cn

## I. INTRODUCTION

Studies of QCD thermodynamics and QCD phase diagram have attracted lots of attentions in recent years. People believe that deconfined quark gluon plasma (QGP) is formed in ultrarelativistic heavy ion collisions [1–8]. Lattice QCD calculations [9–12] as well as models studies [13–21] indicate that there is a critical point in the QCD phase diagram in the plane of temperature and baryon chemical potential [22], which separates the first-order phase transition at high baryon chemical potential from the continuous crossover at high temperature. In the meantime, experiments with the goal to search for the QCD critical point are planned and underway at the Relativistic Heavy Ion Collider (RHIC) at the Brookhaven National Laboratory (BNL) and at the Super Proton Synchrotron (SPS) at CERN in Geneva [23–25]

In order to map the QCD phase diagram, locating the QCD critical point is a crucial and vital task. It has been known that the event-by-event fluctuations of various particle multiplicities are enhanced in heavy ion collisions that freeze out near the critical point. Therefore the QCD critical point can be found through the non-monotonic behavior of various fluctuation observables as a function of varying control parameters [26–35]. Particularly, fluctuations of conserved charges, for example, the baryon number, electric charge, and strangeness, deserve more attentions. On the one hand, the fluctuations of conserved charges are sensitive to the structure of the thermal strongly interacting matter and behave differently between the hadronic and QGP phases [19, 26, 27, 31, 36]. On the other hand, since the conserved charges are conserved through the evolution of the fire ball, the fluctuations of conserved charges can be measured in heavy ion collision experiments.

In our former work [37], we study the fluctuations and correlations of conserved charges in the 2+1 flavor Polyakov–Nambu–Jona-Lasinio (PNJL) model at finite temperature and zero chemical potential. The calculated results are compared with those obtained from recent lattice calculations performed with an improved staggered fermion action at two values of the lattice cutoff with almost physical up and down quark masses and a physical value for the strange quark mass [38]. We find that our calculated results are well consistent with those obtained in lattice calculations, which indicates that the 2+1 flavor PNJL model is valid to be used to study the fluctuations and correlations of conserved charges. The validity of this effective model is expected, since what governs the critical behavior of the

QCD phase transition is the universality class of the chiral symmetry, which is kept in this model. Furthermore, compared with the conventional Nambu–Jona-Lasinio model, the PNJL model not only has the chiral symmetry as well as the dynamical breaking mechanism of this symmetry, but also include the effect of color confinement through the Polyakov loop [21, 39–47].

In this work, we will extend our former work [37] to cases with nonzero baryon chemical potential. This extension is quite nontrivial, because once the baryon chemical potential is nonvanishing, we can use the fluctuations and correlations of conserved charges to explore the critical behavior of the QCD critical point and to find the location of the critical point. Furthermore, when the baryon chemical potential does not vanish, the fluctuations and correlations of odd order develop finite values, which are identical to zero at vanishing baryon chemical potential. In this paper we will pay our most attentions on studies of the non-monotonic behavior of the fluctuations and correlations of conserved charges near the QCD critical point and will depict the contour plots of various fluctuations and correlations in the plane of temperature and baryon chemical potential.

This paper is organized as follows. In Sec. II we introduce the fluctuations and correlations of conserved charges and simply review the formalism of the 2+1 flavor PNJL model. In Sec. III we give our calculated numerical results of the fluctuations of conserved charges. In Sec. IV we give the numerical results of the correlations among conserved charges. In Sec. V we present our summary and conclusions.

## II. FLUCTUATIONS AND CORRELATIONS

In this section we focus on the cumulants of the conserved charge multiplicity distributions, which can be expressed as the derivative of the pressure ( $P$ ) of a thermodynamical system with respect to its chemical potentials corresponding to conserved charges, i.e.

$$\chi_{ijk}^{BQS} = \frac{\partial^{i+j+k}(P/T^4)}{\partial(\mu_B/T)^i \partial(\mu_Q/T)^j \partial(\mu_S/T)^k}, \quad (1)$$

where  $T$  is the temperature, and  $\mu_{B,Q,S}$  are the chemical potentials for baryon number, electric charge, and strangeness, respectively. They are related with the quark chemical potentials through the following relations,

$$\mu_u = \frac{1}{3}\mu_B + \frac{2}{3}\mu_Q, \quad \mu_d = \frac{1}{3}\mu_B - \frac{1}{3}\mu_Q, \quad \text{and} \quad \mu_s = \frac{1}{3}\mu_B - \frac{1}{3}\mu_Q - \mu_S. \quad (2)$$

where  $\mu_{u,d,s}$  are the chemical potentials for  $u$ ,  $d$ , and  $s$  quarks, respectively. Denoting the ensemble average of conserved charge number  $N_X$  ( $X = B, Q, S$ ) with  $\langle N_X \rangle$ , we can obtain the second and higher order fluctuations of the conserved charges as follow

$$\chi_2^X = \frac{1}{VT^3} \langle \delta N_X^2 \rangle, \quad (3)$$

$$\chi_3^X = \frac{1}{VT^3} \langle \delta N_X^3 \rangle, \quad (4)$$

$$\chi_4^X = \frac{1}{VT^3} \left( \langle \delta N_X^4 \rangle - 3 \langle \delta N_X^2 \rangle^2 \right), \quad (5)$$

where  $\delta N_X \equiv N_X - \langle N_X \rangle$  and  $V$  is the volume of the system. In the same way, we can also obtain mixed cumulants of the conserved charge distributions, which are known as the correlations among conserved charges. For example,

$$\chi_{11}^{XY} = \frac{1}{VT^3} \langle \delta N_X \delta N_Y \rangle, \quad (6)$$

$$\chi_{12}^{XY} = \frac{1}{VT^3} \langle \delta N_X \delta N_Y^2 \rangle, \quad (7)$$

$$\chi_{111}^{XYZ} = \frac{1}{VT^3} \langle \delta N_X \delta N_Y \delta N_Z \rangle, \quad (8)$$

It should be noted that when the chemical potentials are vanishing, i.e.  $\mu_{B,Q,S} = 0$ , the fluctuations and correlations of conserved charges in Eq.(1) (also known as generalized susceptibilities) are nonvanishing only when  $i + j + k$  is even, but when  $\mu_B$  has finite values, which are our cases discussed below, the generalized susceptibilities with  $i + j + k$  being odd also develop finite values.

In this work, we employ the 2+1 flavor Polyakov-loop improved NJL model to study the fluctuations and correlations of conserved charges near the QCD critical point. In our former work [37], the fluctuations and correlations of conserved charges are calculated in the 2+1 flavor PNJL model at finite temperature and with vanishing chemical potentials, and the calculated results are well consistent with those obtained in lattice calculations [38], which indicates that the 2+1 flavor PNJL model is valid to study the cumulants of conserved charge multiplicity distributions. In this paper we just give a simple review about the 2+1 flavor PNJL model for completeness. Details about the model can be found in Ref. [21].

The Lagrangian density for the 2+1 flavor PNJL model is given as

$$\begin{aligned} \mathcal{L}_{\text{PNJL}} = & \bar{\psi}(i\gamma_\mu D^\mu + \gamma_0 \hat{\mu} - \hat{m}_0)\psi + G \sum_{a=0}^8 \left[ (\bar{\psi} \tau_a \psi)^2 + (\bar{\psi} i\gamma_5 \tau_a \psi)^2 \right] \\ & - K \left[ \det_f(\bar{\psi}(1 + \gamma_5)\psi) + \det_f(\bar{\psi}(1 - \gamma_5)\psi) \right] - \mathcal{U}(\Phi, \Phi^*, T), \end{aligned} \quad (9)$$

where  $\psi = (\psi_u, \psi_d, \psi_s)^T$  is the three-flavor quark field, and

$$D^\mu = \partial^\mu - iA^\mu \quad \text{with} \quad A^\mu = \delta_0^\mu A^0 \quad , \quad A^0 = g\mathcal{A}_a^0 \frac{\lambda_a}{2} = -iA_4, \quad (10)$$

where  $\lambda_a$ 's are the Gell-Mann matrices in color space and  $g$  is the gauge coupling strength.  $\hat{m}_0 = \text{diag}(m_0^u, m_0^d, m_0^s)$  is the three-flavor current quark mass matrix. Throughout this work, we take  $m_0^u = m_0^d \equiv m_0^l$ , while keep  $m_0^s$  being larger than  $m_0^l$ , which breaks the  $SU(3)_f$  symmetry. In matrix  $\hat{\mu} = \text{diag}(\mu_u, \mu_d, \mu_s)$  are the quark chemical potentials which are related with the conserved charge chemical potentials through relations in Eq.(2).

In the above PNJL Lagrangian,  $\mathcal{U}(\Phi, \Phi^*, T)$  is the Polyakov-loop effective potential, which is expressed in terms of the traced Polyakov-loop  $\Phi = (\text{Tr}_c L)/N_c$  and its conjugate  $\Phi^* = (\text{Tr}_c L^\dagger)/N_c$  with the Polyakov-loop  $L$  being a matrix in color space given explicitly by

$$L(\vec{x}) = \mathcal{P} \exp \left[ i \int_0^\beta d\tau A_4(\vec{x}, \tau) \right] = \exp[i\beta A_4], \quad (11)$$

with  $\beta = 1/T$  being the inverse of temperature and  $A_4 = iA^0$ .

In our work, we use the Polyakov-loop effective potential which is a polynomial in  $\Phi$  and  $\Phi^*$  [42], given by

$$\frac{\mathcal{U}(\Phi, \Phi^*, T)}{T^4} = -\frac{b_2(T)}{2} \Phi^* \Phi - \frac{b_3}{6} (\Phi^3 + \Phi^{*3}) + \frac{b_4}{4} (\Phi^* \Phi)^2, \quad (12)$$

with

$$b_2(T) = a_0 + a_1 \left( \frac{T_0}{T} \right) + a_2 \left( \frac{T_0}{T} \right)^2 + a_3 \left( \frac{T_0}{T} \right)^3. \quad (13)$$

Parameters in the effective potential are fitted to reproduce the thermodynamical behavior of the pure-gauge QCD obtained from the lattice simulations, and their values are given in Table I. The parameter  $T_0$  is the critical temperature for the deconfinement phase transition to take place in pure-gauge QCD and  $T_0$  is chosen to be 270 MeV according to the lattice calculations.

TABLE I: Parameters for the Polyakov-loop effective potential  $\mathcal{U}$

$a_0$	$a_1$	$a_2$	$a_3$	$b_3$	$b_4$
6.75	-1.95	2.625	-7.44	0.75	7.5

In the mean field approximation, the thermodynamical potential density for the 2+1 flavor quark system is given by

$$\begin{aligned}
\Omega = & -2N_c \sum_{f=u,d,s} \int \frac{d^3p}{(2\pi)^3} \left\{ E_p^f \theta(\Lambda^2 - p^2) \right. \\
& + \frac{T}{3} \ln [1 + 3\Phi^* e^{-(E_p^f - \mu_f)/T} + 3\Phi e^{-2(E_p^f - \mu_f)/T} + e^{-3(E_p^f - \mu_f)/T}] \\
& + \frac{T}{3} \ln [1 + 3\Phi e^{-(E_p^f + \mu_f)/T} + 3\Phi^* e^{-2(E_p^f + \mu_f)/T} + e^{-3(E_p^f + \mu_f)/T}] \left. \right\} \\
& + 2G(\phi_u^2 + \phi_d^2 + \phi_s^2) - 4K\phi_u\phi_d\phi_s + \mathcal{U}(\Phi, \Phi^*, T),
\end{aligned} \tag{14}$$

where  $\phi_i$ 's ( $i = u, d, s$ ) are the quark chiral condensates, and the energy-momentum dispersion relation is  $E_p^i = \sqrt{p^2 + M_i^2}$ , with the constituent mass being

$$M_i = m_0^i - 4G\phi_i + 2K\phi_j\phi_k. \tag{15}$$

Minimizing the thermodynamical potential in Eq. (14) with respect to  $\phi_u, \phi_d, \phi_s, \Phi$ , and  $\Phi^*$ , we obtain a set of equations of motion. Then, these equations can be solved as functions of temperature  $T$  and three conserved charge chemical potentials  $\mu_B, \mu_Q$ , and  $\mu_S$ .

In this work we use the method of Taylor expansion to compute the fluctuations and correlations of conserved charges in the PNJL model. Before our numerical calculations, we should determine the five parameters in the quark sector of the model. Values of the five parameters used usually in the literatures are obtained in Ref. [48], which are  $m_0^l = 5.5$  MeV,  $m_0^s = 140.7$  MeV,  $G\Lambda^2 = 1.835$ ,  $K\Lambda^5 = 12.36$ , and  $\Lambda = 602.3$  MeV. They are fixed by fitting  $m_\pi = 135.0$  MeV,  $m_K = 497.7$  MeV,  $m_{\eta'} = 957.8$  MeV, and  $f_\pi = 92.4$  MeV.

### III. NUMERICAL RESULTS OF FLUCTUATIONS OF CONSERVED CHARGES

In this section, we give our calculated results of the conserved charge fluctuations in the 2+1 flavor PNJL model. We find that the QCD critical point is located at about  $T_c = 160$  MeV and  $\mu_{B_c} = 819$  MeV ( $\mu_Q = \mu_S = 0$ ) with parameters given above. This QCD critical point separates the first-order chiral phase transition at high baryon chemical potential from the continuous crossover at high temperature. Our attentions are paid to study the behaviors of the conserved charge fluctuations near the critical point, especial their singular behaviors, which shed light on the universal symmetry property of the QCD critical point. Furthermore, the singular behaviors of conserved charge fluctuations are also

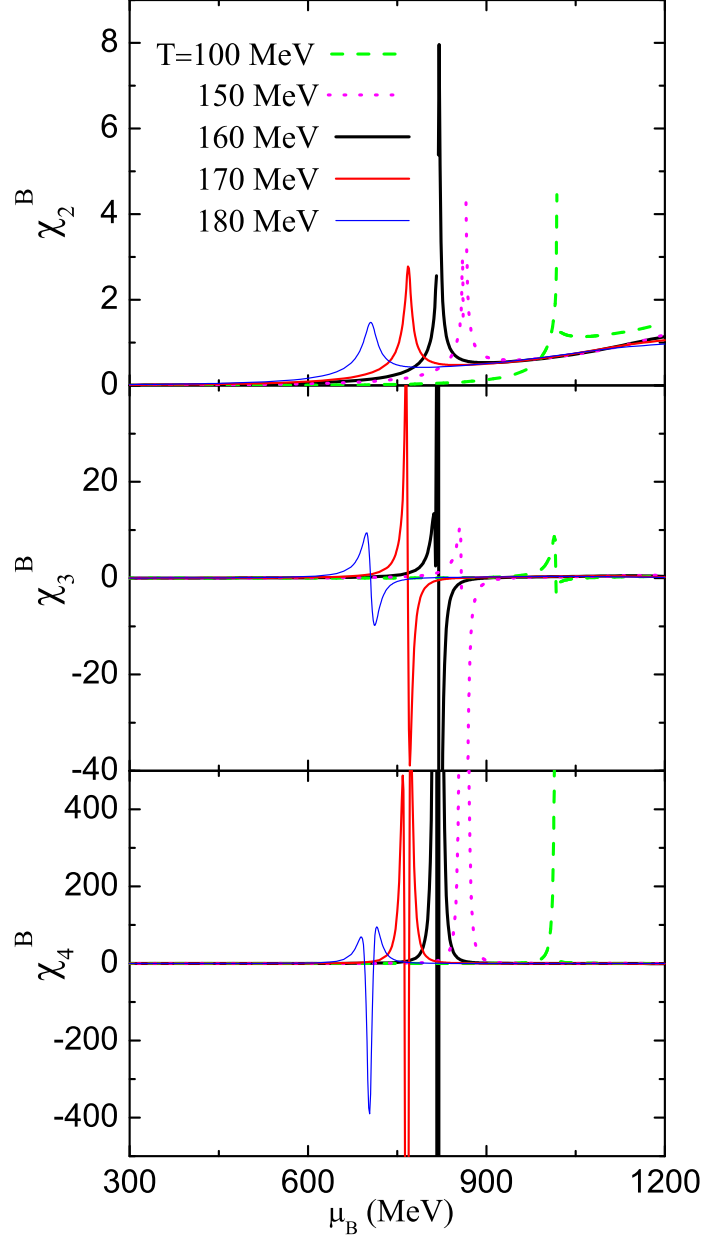


FIG. 1: (color online). Quadratic (top), cubic (middle), and quartic (bottom) fluctuations of baryon number as functions of the baryon chemical potential  $\mu_B$  ( $\mu_Q = \mu_S = 0$ ) with several values of temperature in the PNJL model.

very helpful for searching for the QCD critical point in experiments [35]. In Fig. 1 we show the quadratic, cubic, and quartic fluctuations of baryon number as functions of  $\mu_B$  ( $\mu_Q = \mu_S = 0$ ) at several values of temperature calculated in the PNJL model. From the top panel of Fig. 1 one can find that  $\chi_2^B$  has a peak structure when the chiral phase transition

takes place, and this peak becomes sharper and narrower while moving toward the QCD critical point. We can also clearly find that the  $\chi_2^B$  diverges at the critical point, seeing the curve corresponding to temperature of 160 MeV. According to the definition of cumulants of the conserved charge multiplicity distributions in Eq.(1), we have  $\chi_3^B = \partial\chi_2^B/\partial(\mu_B/T)$ . Since  $\chi_2^B$  develops a cusp during the chiral phase transition,  $\chi_3^B$  changes its sign there, which is clearly shown in the middle panel of Fig. 1. This structure of  $\chi_3^B$  is also found by Asakawa et al. [33], who argue that the two sides of the QCD phase boundary can be distinguished by the sign of  $\chi_3^B$ , therefore the third cumulants carry more information than the second ones. One can also find that  $\chi_3^B$  diverges at the QCD critical point. Furthermore, we also calculate the fourth-order fluctuations of the baryon number, and the results are shown in the bottom panel of Fig. 1. Along the analysis above, One can expect that  $\chi_4^B$  carries even more information than  $\chi_3^B$ , since  $\chi_4^B$  has two positive maxima and one negative minimum as Fig. 1 shows. Furthermore, we find that all amplitudes of  $\chi_2^B$ ,  $\chi_3^B$ , and  $\chi_4^B$  grows rapidly when moving toward the QCD critical point and finally diverge there.

In Fig. 2 we plot contours of the quadratic, cubic, and quartic fluctuations of the baryon number as functions of  $T$  and  $\mu_B$  calculated in the PNJL model. One can clearly find that the chiral phase transition line in each of the three contour plots is obvious, and more important is that the region near around the QCD critical point can also be found in the three plots, where the contour lines are dense. Therefore, our calculations indicate that employing the second and higher order cumulants of baryon multiplicity distributions to search for the QCD critical point is possible. We should emphasize that in heavy ion collision experiments finite size and finite time effects should also be included [29, 35]. Comparing higher order cumulants  $\chi_3^B$  and  $\chi_4^B$  with the quadratic one  $\chi_2^B$ , we find that the former are superior to the latter in the search for the QCD critical point, because only when the location is very near the chiral phase transition line,  $\chi_3^B$  and  $\chi_4^B$  are nonvanishing, while  $\chi_2^B$  still has finite value when the location is far from the chiral phase transition line and in the chiral symmetry restored phase as the top panel of Fig. 2 shows.

In Fig. 3 we show  $\chi_3^B/\chi_2^B$  and  $\chi_4^B/\chi_2^B$  versus baryon chemical potential at several values



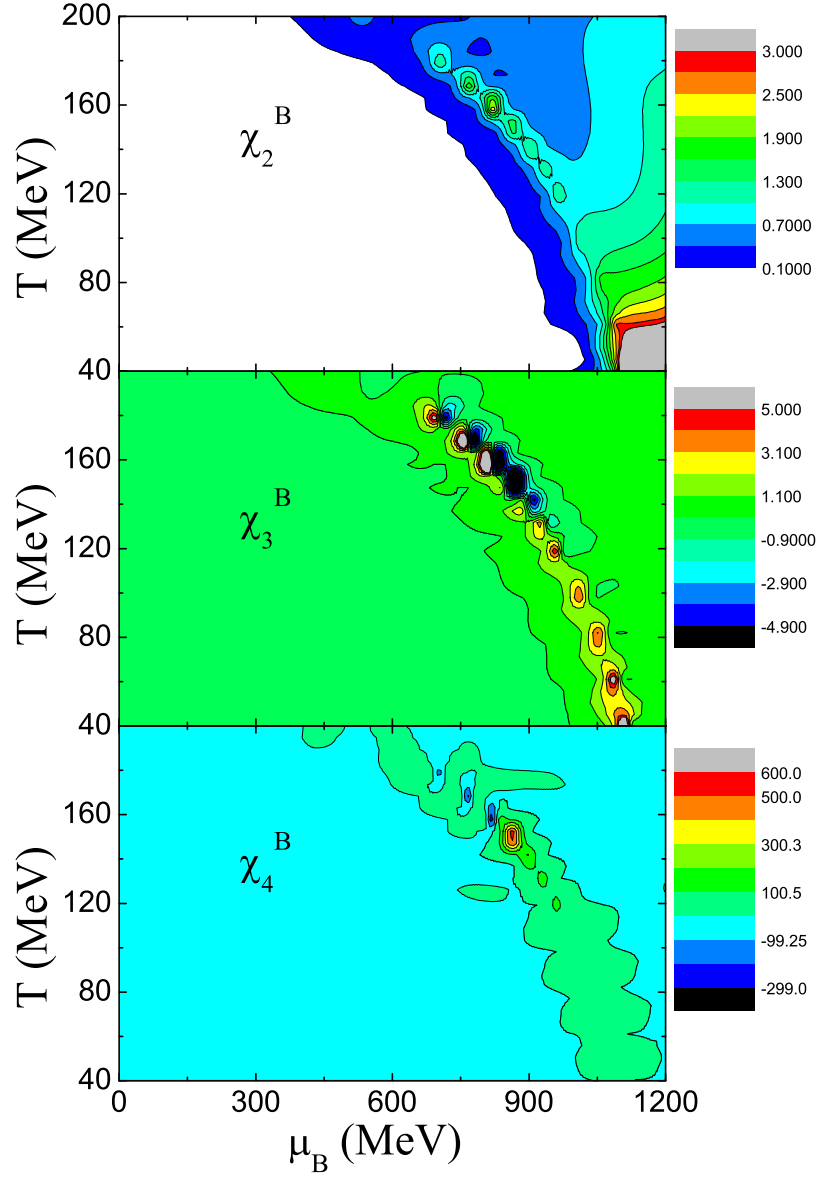


FIG. 2: (color online). Contour plots of quadratic (top), cubic (middle), and quartic (bottom) fluctuations of the baryon number as functions of temperature  $T$  and baryon chemical potential  $\mu_B$  ( $\mu_Q = \mu_S = 0$ ) in the PNJL model.

of temperature calculated in the PNJL model. From Eq.(3) to Eq.(5) we find

$$\frac{\chi_3^B}{\chi_2^B} = \frac{\langle \delta N_B^3 \rangle}{\langle \delta N_B^2 \rangle}, \quad (16)$$

$$\frac{\chi_4^B}{\chi_2^B} = \frac{\langle \delta N_B^4 \rangle - 3\langle \delta N_B^2 \rangle^2}{\langle \delta N_B^2 \rangle}. \quad (17)$$

In fact,  $\chi_3^B/\chi_2^B$  and  $\chi_4^B/\chi_2^B$  are the skewness and kurtosis of the baryon multiplicity distri-

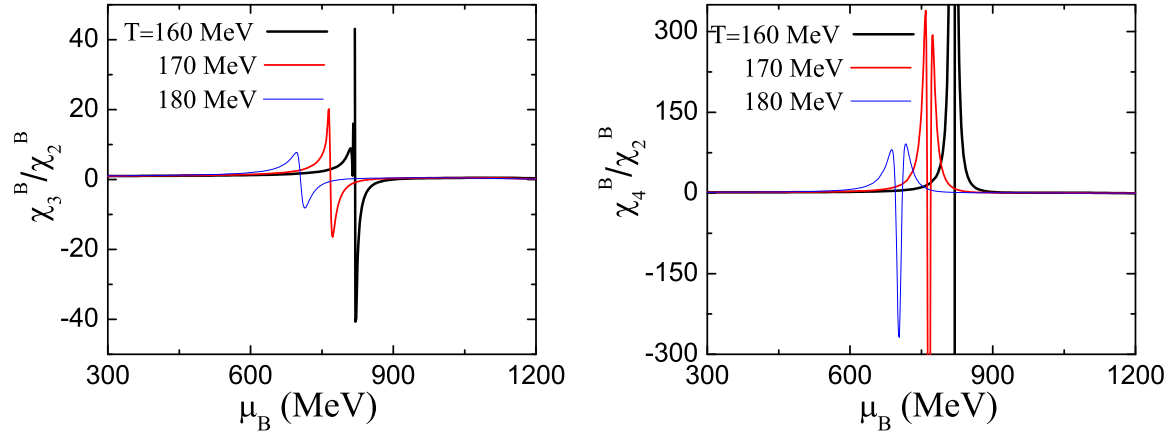


FIG. 3: (color online). Ratios of cubic to quadratic (left panel) and those of quartic to quadratic (right panel) baryon number fluctuations as functions of baryon chemical potential  $\mu_B$  ( $\mu_Q = \mu_S = 0$ ) at several values of temperature in the PNJL model.

butions, respectively, which can be extracted from event-by-event fluctuations in heavy ion collision experiments. Furthermore, these ratios are intensive quantities, i.e., being independent of the volume of the system. In Fig. 3 we find that  $\chi_3^B/\chi_2^B$  and  $\chi_4^B/\chi_2^B$  have the same structure as  $\chi_3^B$  and  $\chi_4^B$ , respectively, i.e.,  $\chi_3^B/\chi_2^B$  change its sign during the chiral phase transition and there are two positive maxima and one negative minimum on  $\chi_4^B/\chi_2^B$ . Furthermore, we also find that the amplitudes of  $\chi_3^B/\chi_2^B$  and  $\chi_4^B/\chi_2^B$  grow rapidly when moving toward the QCD critical point and they diverge there.

Fig. 4 shows the quadratic, cubic, and quartic cumulants of the electric charge multiplicity distributions as functions of  $\mu_B$  calculated in the PNJL model. We find that  $\chi_2^Q$  increases with the baryon chemical potential and it has a cusp during the chiral phase transition. Comparing  $\chi_2^Q$  with  $\chi_2^B$ , we find that the peak in  $\chi_2^Q$  grows less rapidly than that in  $\chi_2^B$ . As for higher order fluctuations of the electric charge, we find that  $\chi_3^Q$  changes its sign during the chiral phase transition and  $\chi_4^Q$  has two maxima and one minimum, which are same with  $\chi_3^B$  and  $\chi_4^B$ , respectively. We should emphasize that once the location deviates from the chiral phase transition line, the higher order fluctuations of electric charge approach zero rapidly, while the second-order fluctuation  $\chi_2^Q$  still has finite value even the location is far away from the chiral phase transition line.

In Fig. 5 we show the contour plots of the quadratic, cubic, and quartic fluctuations of electric charge as functions of temperature and baryon chemical potential calculated in the

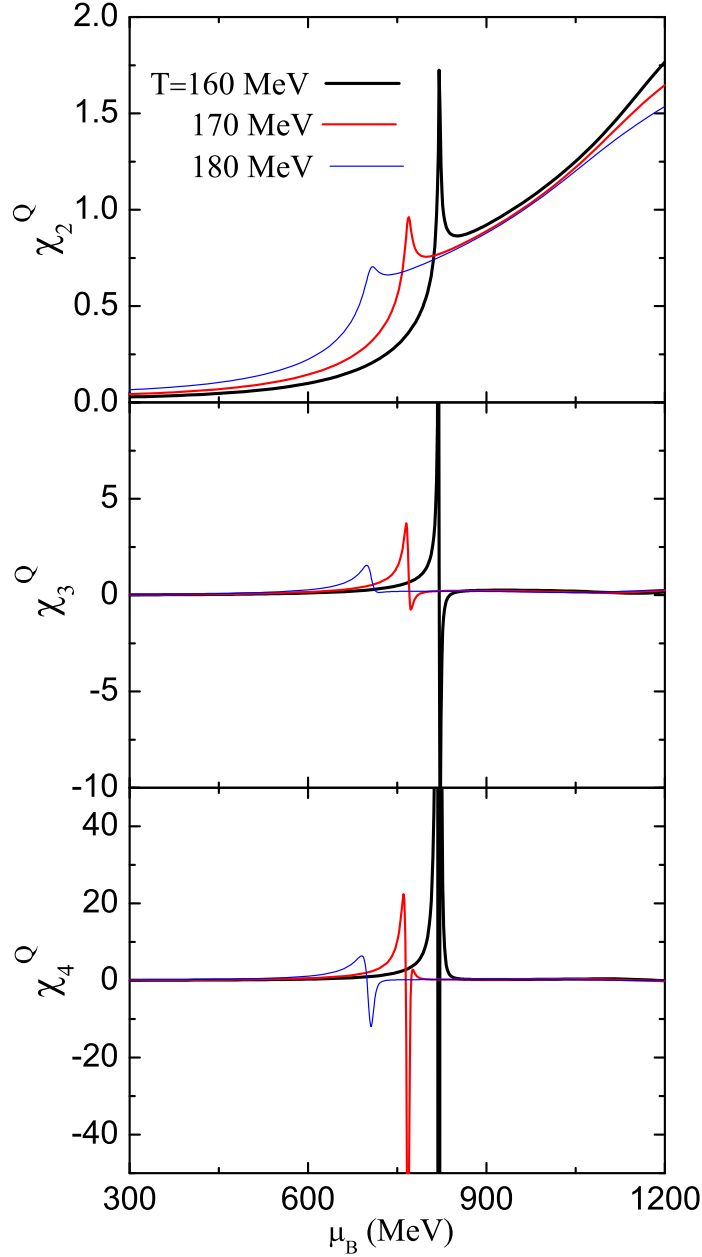


FIG. 4: (color online). Quadratic (top), cubic (middle), and quartic (bottom) fluctuations of electric charge as functions of baryon chemical potential  $\mu_B$  ( $\mu_Q = \mu_S = 0$ ) with several values of temperature in the PNJL model.

PNJL model. In the three plots one can recognize the chiral phase transition line easily, same as the contour plots of baryon number fluctuations in Fig. 2. However, we find that employing the quadratic fluctuations of electric charge to search for the QCD critical point is not easy, as the top panel of Fig. 5 show that the critical point in this plot is not obvious.

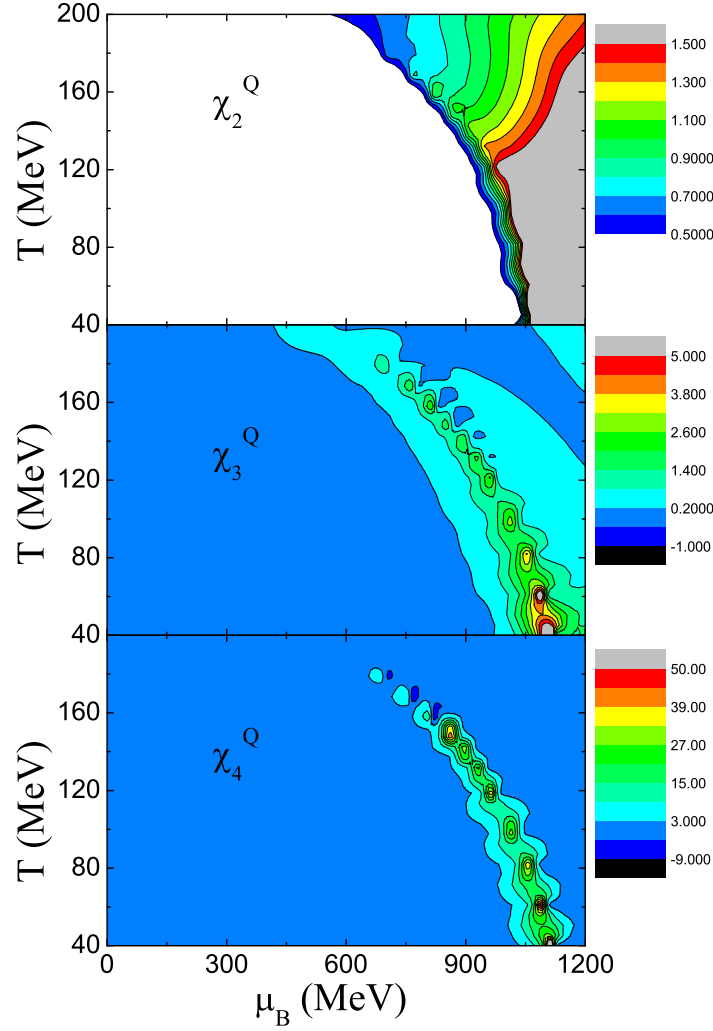


FIG. 5: (color online). Contour plots of quadratic (top), cubic (middle), and quartic (bottom) fluctuations of electric charge as functions of temperature  $T$  and baryon chemical potential  $\mu_B$  ( $\mu_Q = \mu_S = 0$ ) in the PNJL model.

While for the higher order fluctuations of electric charge, one can find that the QCD critical point in the contour plots of  $\chi_3^Q$  and  $\chi_4^Q$  is distinct. Therefore, higher order fluctuations of electric charge are more appropriate for being used to search for the QCD critical point in heavy ion collision experiments.

Fig. 6 shows the quadratic, cubic, and quartic fluctuations of strangeness versus the baryon chemical potential at several values of temperature calculated in the PNJL model. We find that the second-order and higher order fluctuations of strangeness are also enhanced when moving toward the QCD critical point, which are same as the fluctuations of baryon

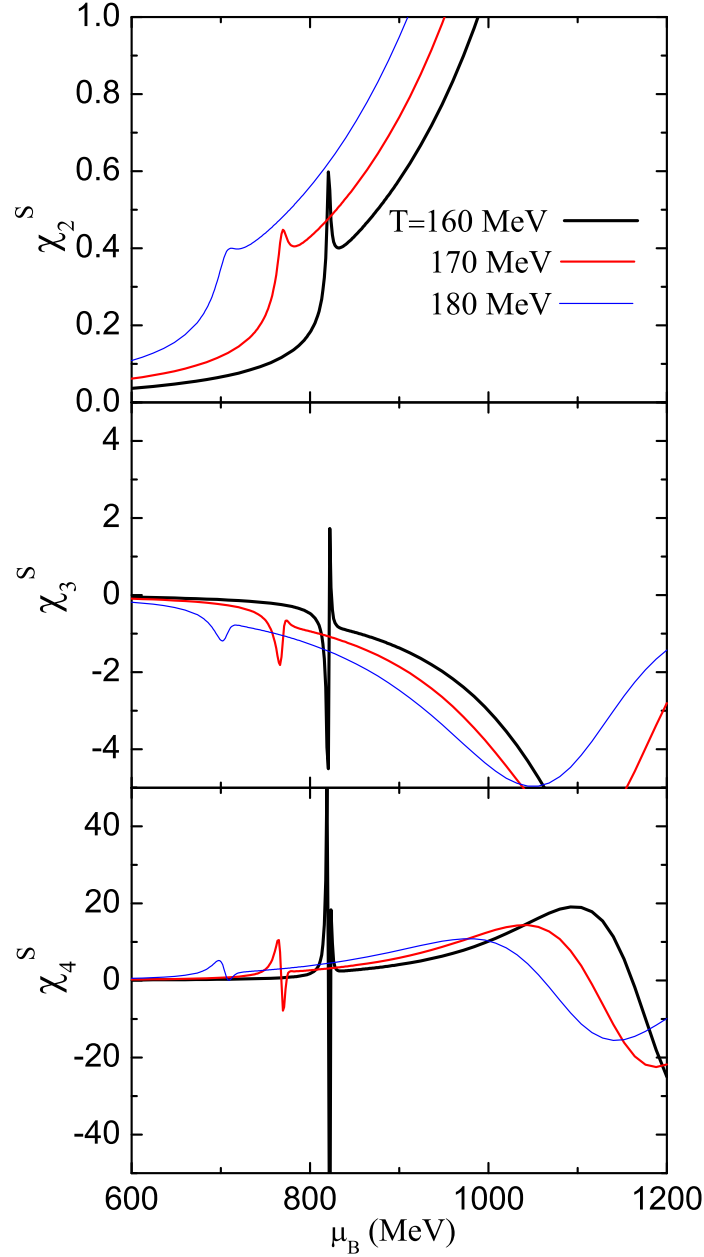


FIG. 6: (color online). Quadratic (top), cubic (middle), and quartic (bottom) fluctuations of strangeness as functions of baryon chemical potential  $\mu_B$  ( $\mu_Q = \mu_S = 0$ ) with several values of temperature in the PNJL model.

number and electric charge. However, contributions to the singularity of the strangeness fluctuations from the QCD critical point are less than those to the baryon number or electric charge fluctuations. In the same way, we find that higher order fluctuations of strangeness are superior to the second-order one in search for the QCD critical point.

#### IV. NUMERICAL RESULTS OF CORRELATIONS OF CONSERVED CHARGES

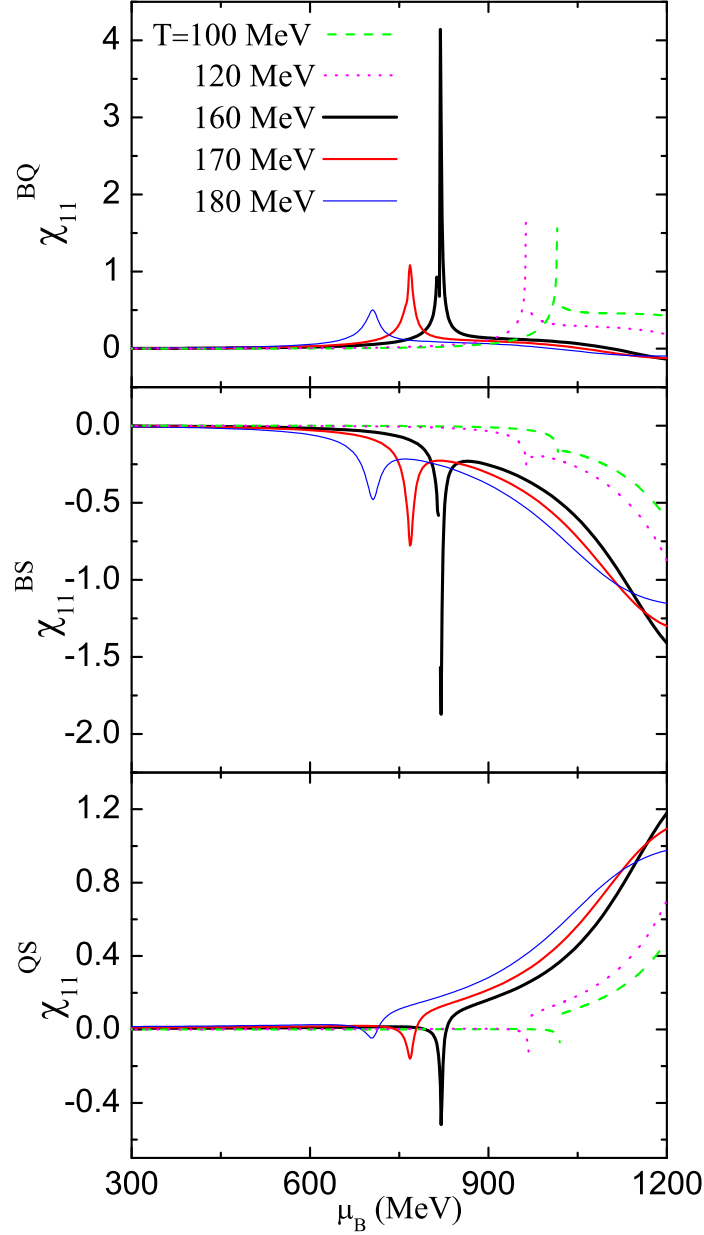


FIG. 7: (color online). Second-order correlations between baryon number and electric charge (top), baryon number and strangeness (middle), electric charge and strangeness (bottom) as functions of the baryon chemical potential  $\mu_B$  ( $\mu_Q = \mu_S = 0$ ) with several values of temperature in the PNJL model.

In this section, we give our calculated results of the correlations between or among con-

served charges in the 2+1 flavor PNJL model. We will show that higher order correlations of conserved charges are sensitive to the critical behaviors related to the QCD critical point and therefore are very appropriate for being employed to search for the critical point. In Fig. 7 we show the dependence of the second-order correlations, i.e.,  $\chi_{11}^{BQ}$ ,  $\chi_{11}^{BS}$ , and  $\chi_{11}^{QS}$  on the baryon chemical potential at several values of temperature in the PNJL model. We find that all the second-order correlations have a non-monotonic behavior as functions of the baryon chemical potential. There is a peak structure on  $\chi_{11}^{BQ}$  during the chiral phase transition;  $\chi_{11}^{BS}$  is negative in the whole chemical potential region and has a minimum at the phase transition; and  $\chi_{11}^{QS}$  also has a negative minimum but its value is positive in the chiral symmetry restored phase. Comparing  $\chi_{11}^{BQ}$  with  $\chi_{11}^{BS}$  and  $\chi_{11}^{QS}$  one can find that  $\chi_{11}^{BQ}$  does not vanish only when the thermodynamical system is very near the chiral phase transition, while the magnitude of  $\chi_{11}^{BS}$  and  $\chi_{11}^{QS}$  increases with the baryon chemical potential in the chiral symmetric phase as the middle and bottom panels of Fig. 7 show. These are because in the chiral symmetric phase, the system can be approximated as noninteracting massless gases, i.e., the Stefan-Boltzmann limit. It can be easily shown that in the Stefan-Boltzmann limit  $\chi_{11}^{BQ}$  is vanishing while  $\chi_{11}^{BS}$  and  $\chi_{11}^{QS}$  have finite values [37].

Fig. 8 gives the contour plots of the second-order correlations  $\chi_{11}^{BQ}$ ,  $\chi_{11}^{BS}$ , and  $\chi_{11}^{QS}$  as functions of temperature and baryon chemical potential calculated in the PNJL model. One can find that the chiral phase transition line in the three plots is distinct, but the QCD critical point in the plot of  $\chi_{11}^{BQ}$  is more apparent than that in  $\chi_{11}^{BS}$  or  $\chi_{11}^{QS}$ .

In Fig. 9 we show the third-order correlations  $\chi_{21}^{BQ}$ ,  $\chi_{12}^{BQ}$ ,  $\chi_{21}^{BS}$ ,  $\chi_{12}^{BS}$ ,  $\chi_{21}^{QS}$ , and  $\chi_{12}^{QS}$  as functions of the baryon chemical potential at several values of temperature calculated in the PNJL model. We find that all these third-order correlations change their signs at the chiral phase transition, which are same as the third-order fluctuations of conserved charges. More concretely,  $\chi_{21}^{BS}$  and  $\chi_{21}^{QS}$  change their signs from negative to positive with the increase of the baryon chemical potential during the chiral phase transition, while other correlations in Fig. 9 change their signs in the opposite direction. Furthermore, one can find that the oscillating amplitudes of these third-order correlations all increase rapidly when moving toward the QCD critical point and they diverge there.

Fig. 10 shows the contour plots of the third-order correlations  $\chi_{21}^{BQ}$ ,  $\chi_{12}^{BQ}$ ,  $\chi_{21}^{BS}$ ,  $\chi_{12}^{BS}$ ,  $\chi_{21}^{QS}$ , and  $\chi_{12}^{QS}$  as functions of temperature and baryon chemical potential calculated in the PNJL model. Comparing Fig. 10 and Fig. 8, one can easily find that the QCD critical

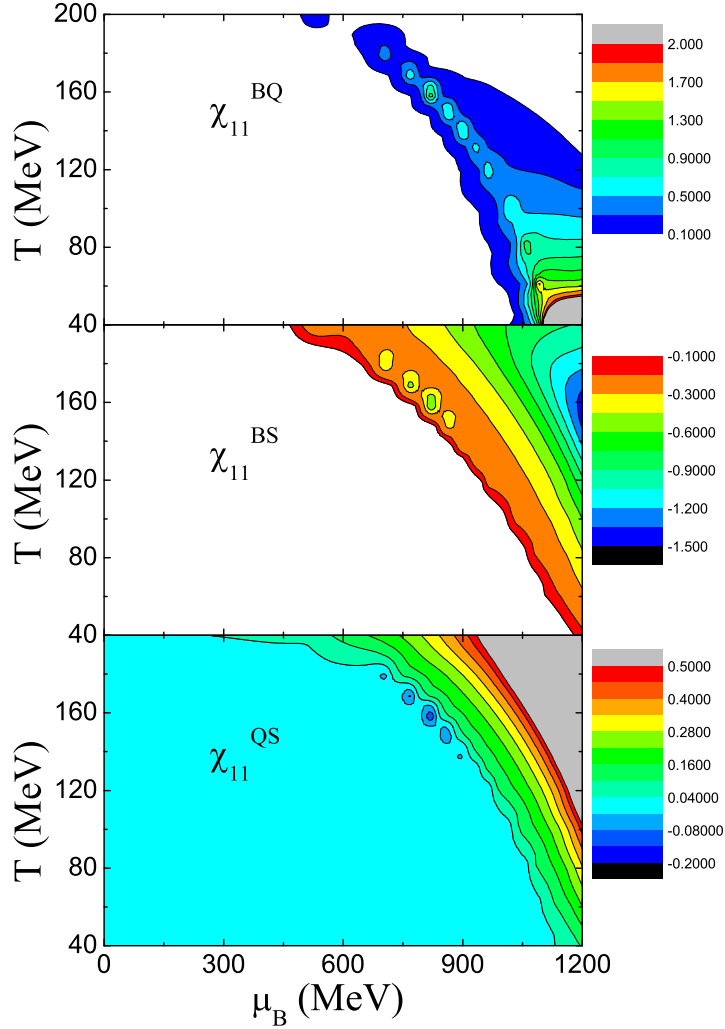


FIG. 8: (color online). Contour plots of the second-order correlations  $\chi_{11}^{BQ}$  (top),  $\chi_{11}^{BS}$  (middle), and  $\chi_{11}^{QS}$  (bottom) as functions of temperature  $T$  and baryon chemical potential  $\mu_B$  ( $\mu_Q = \mu_S = 0$ ) in the PNJL model.

point in Fig. 10 is much more obvious than that in Fig. 8, which means that higher order correlations are more sensitive to the critical behavior of the QCD critical point than the quadratic correlations, and are better to be used as probes to explore the critical behavior of the QCD critical point in heavy ion collision experiments. As for the six contour plots in Fig. 10, we find that the QCD critical point in  $\chi_{21}^{BQ}$ ,  $\chi_{21}^{BS}$ , and  $\chi_{21}^{QS}$  is more distinct than that in  $\chi_{12}^{BQ}$ ,  $\chi_{12}^{BS}$ , and  $\chi_{12}^{QS}$ .

In Fig. 11 we show the last third-order correlation  $\chi_{111}^{BQS}$ , i.e., the correlation among the baryon number, electric charge, and the strangeness, as function of the baryon chemical po-



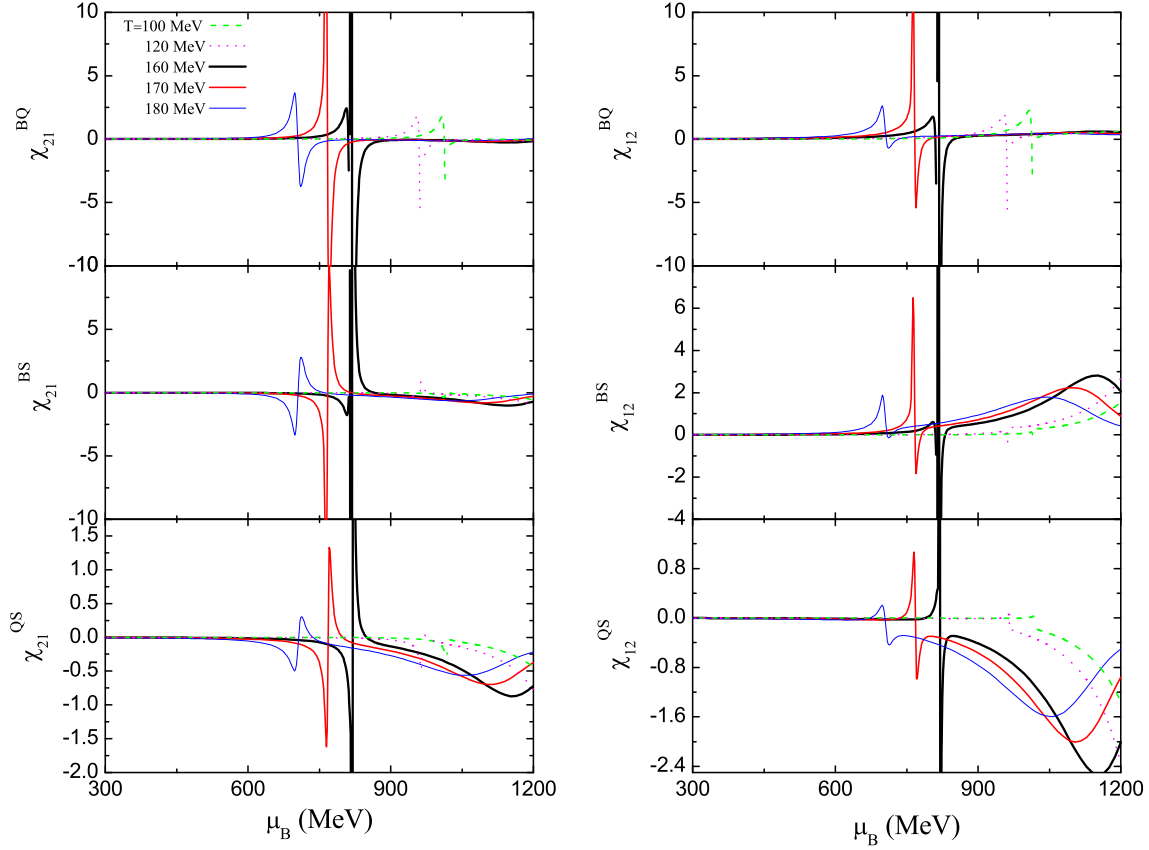


FIG. 9: (color online). Third-order correlations  $\chi_{21}^{BQ}$  (top-left),  $\chi_{12}^{BQ}$  (top-right),  $\chi_{21}^{BS}$  (middle-left),  $\chi_{12}^{BS}$  (middle-right),  $\chi_{21}^{QS}$  (bottom-left), and  $\chi_{12}^{QS}$  (bottom-right) as functions of the baryon chemical potential  $\mu_B$  ( $\mu_Q = \mu_S = 0$ ) with several values of temperature in the PNJL model.

tential with several values of temperature calculated in the PNJL model. We find that  $\chi_{111}^{BQS}$  changes its sign from negative to positive during the chiral phase transition and diverges at the QCD critical point. Furthermore, one can find that only when the thermodynamical system is near the chiral phase transition,  $\chi_{111}^{BQS}$  has nonvanishing value. In the same way, we show the corresponding contour plot of the  $\chi_{111}^{BQS}$  as function of  $T$  and  $\mu_B$  in Fig. 12. As Fig. 12 shows, the QCD critical point in the contour plot of  $\chi_{111}^{BQS}$  is very obvious. Therefore,  $\chi_{111}^{BQS}$  is an ideal probe to search for the QCD critical point in heavy ion collision experiments.

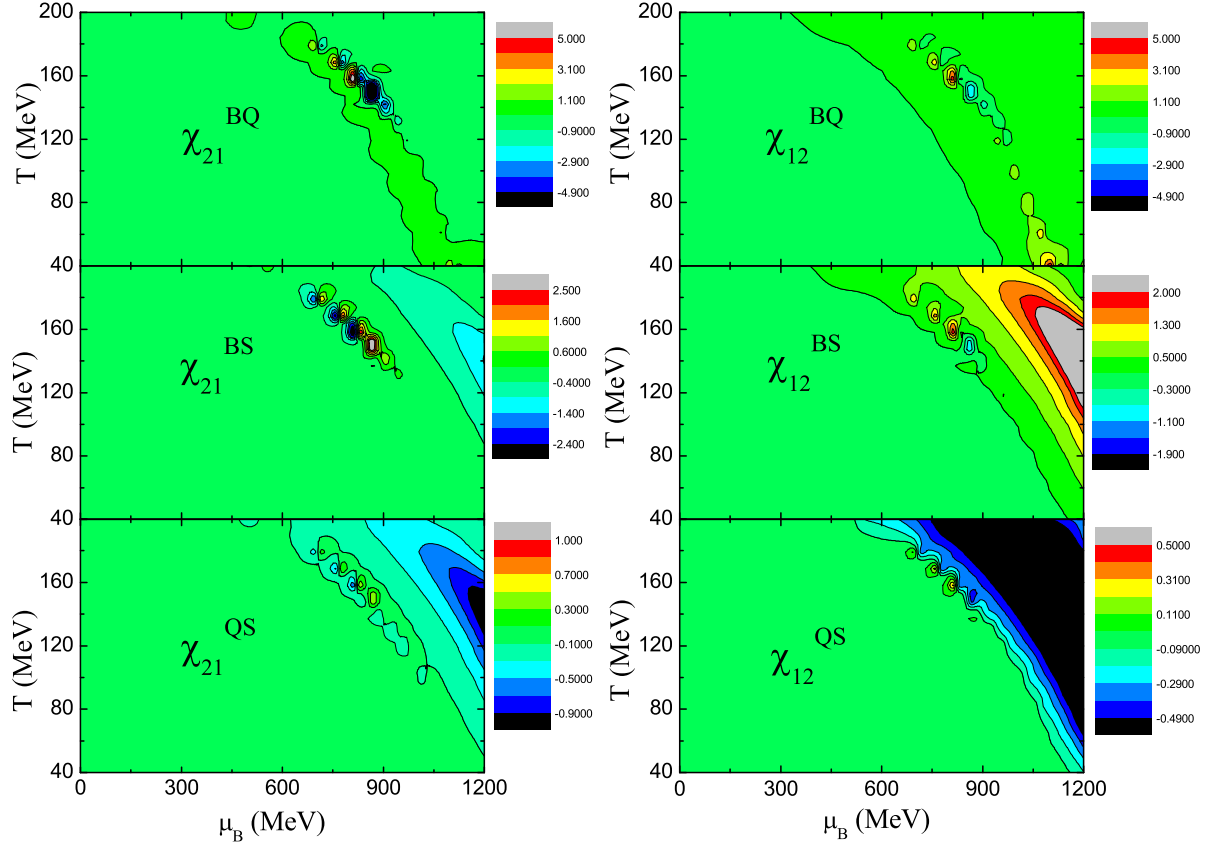


FIG. 10: (color online). Contour plots of the third-order correlations  $\chi_{21}^{BQ}$  (top-left),  $\chi_{12}^{BQ}$  (top-right),  $\chi_{21}^{BS}$  (middle-left),  $\chi_{12}^{BS}$  (middle-right),  $\chi_{21}^{QS}$  (bottom-left), and  $\chi_{12}^{QS}$  (bottom-right) as functions of temperature  $T$  and baryon chemical potential  $\mu_B$  ( $\mu_Q = \mu_S = 0$ ) in the PNJL model.

## V. SUMMARY AND DISCUSSIONS

In this work, we have studied the fluctuations and correlations of conserved charges, i.e. the baryon number, electric charge and the strangeness, in the 2+1 flavor Polyakov–Nambu–Jona-Lasinio model at finite temperature and nonzero baryon chemical potential. More attentions are paid on studies of the non-monotonic behavior of the fluctuations and correlations of conserved charges near the QCD critical point. The fluctuations are calculated up to the fourth-order and the correlations to the third-order.

We find that the second-order fluctuations and correlations have a peak or valley structure when the chiral phase transition takes place with the increase of the baryon chemical

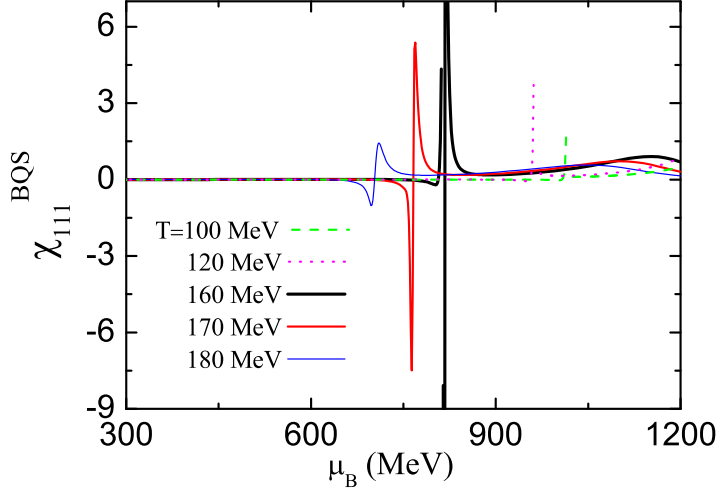


FIG. 11: (color online). Third-order correlation among baryon number, electric charge, and strangeness, i.e.,  $\chi_{111}^{BQS}$  as function of the baryon chemical potential  $\mu_B$  ( $\mu_Q = \mu_S = 0$ ) with several values of temperature in the PNJL model.

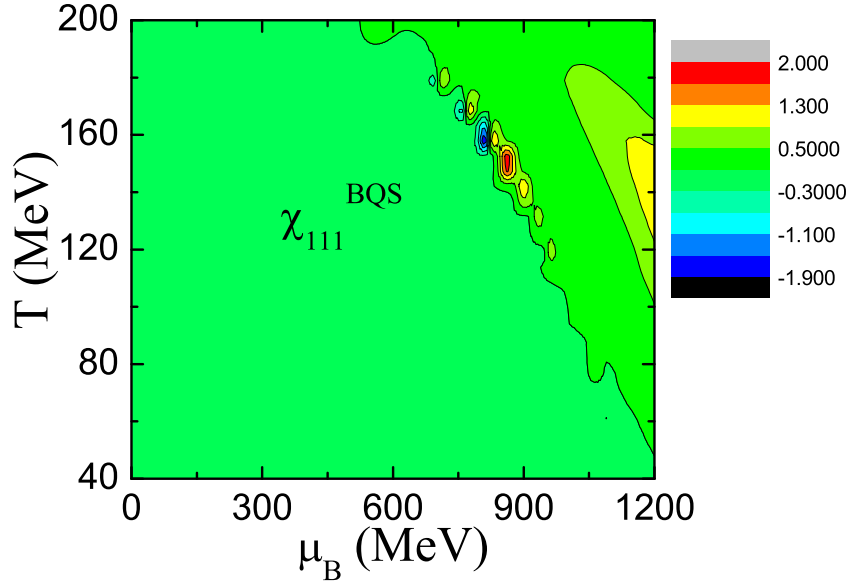


FIG. 12: (color online). Contour plot of the third-order correlation  $\chi_{111}^{BQS}$  as function of temperature  $T$  and baryon chemical potential  $\mu_B$  ( $\mu_Q = \mu_S = 0$ ) in the PNJL model.

potential. As for the higher order fluctuations and correlations of conserved charges, we find that the third-order fluctuations and correlations change their signs during the chiral

phase transition and the fourth-order fluctuations have two maximum and one minimum. Furthermore, the extrema of the fluctuations and correlations at the chiral phase transition increase rapidly when the thermodynamical system moves toward the QCD critical point (in heavy ion collision experiments these mean that the freeze-out point moves toward the QCD critical point), and finally the fluctuations and correlations of conserved charges diverge at the critical point.

In this work we also depict contour plots of the fluctuations and correlations of conserved charges. In these contour plots one can clearly find the chiral phase transition line. Comparing with the second-order fluctuations and correlations, we find that higher order cumulants, which in this paper are the third- and fourth-order fluctuations and the third-order correlations, are more sensitive to the critical behavior of the QCD critical point. Therefore, higher order fluctuations and correlations of conserved charges are superior to the second-order ones to be used to search for the critical point in heavy ion collision experiments. Particularly, we should point out that among all the fluctuations and correlations studied in this paper, the calculations in the 2+1 flavor PNJL model indicate that  $\chi_{21}^{BQ}$ ,  $\chi_{21}^{BS}$ ,  $\chi_{21}^{QS}$ , and  $\chi_{111}^{BQS}$  are the most valuable probes to search for the QCD critical point.

### Acknowledgements

One of the authors (W. J. F.) acknowledges financial support from China Postdoctoral Science Foundation No. 20090460534.

- 
- [1] E. V. Shuryak, Prog. Part. Nucl. Phys. **53**, 273 (2004).
  - [2] M. Gyulassy, and L. McLerran, Nucl. Phys. **A 750**, 30 (2005).
  - [3] E. V. Shuryak, Nucl. Phys. **A 750**, 64 (2005).
  - [4] I. Arsene *et al*, Nucl. Phys. **A 757**, 1 (2005).
  - [5] B. B. Back *et al*, Nucl. Phys. **A 757**, 28 (2005).
  - [6] J. Adams *et al*, Nucl. Phys. **A 757**, 102 (2005).
  - [7] K. Adcox *et al*, Nucl. Phys. **A 757**, 184 (2005).
  - [8] J.-P. Blaizot, J. Phys. **G 34**, S243 (2007).

- [9] Z. Fodor, and S. D. Katz, Phys. Lett. **B 534**, 87 (2002); *ibid*, J. High Energy Phys. **0203**, 014 (2002); Z. Fodor, S. D. Katz, and K. K. Szabo, Phys. Lett. **B 568**, 73 (2003).
- [10] S. Ejiri, C. R. Allton, S. J. Hands, O. Kaczmarek, F. Karsch, E. Laermann and C. Schmidt, Prog. Theor. Phys. Suppl. **153**, 118 (2004).
- [11] R. V. Gavai and S. Gupta, Phys. Rev. **D 71**, 114014 (2005).
- [12] P. de Forcrand, and O. Philipsen, Nucl. Phys. **B 642**, 290 (2002); **B 673**, 170 (2003); P. de Forcrand, and S. Kratochvila, Nucl. Phys. B, Proc. Suppl. **153**, 62 (2006).
- [13] M. Asakawa and K. Yazaki, Nucl. Phys. **A 504**, 668 (1989).
- [14] A. Barducci, R. Casalbuoni, S. De Curtis, R. Gatto and G. Pettini, Phys. Lett. **B 231**, 463 (1989); Phys. Rev. **D 41**, 1610 (1990).
- [15] A. Barducci, R. Casalbuoni, G. Pettini and R. Gatto, Phys. Rev. **D 49**, 426 (1994).
- [16] J. Berges and K. Rajagopal, Nucl. Phys. **B 538**, 215 (1999).
- [17] M. A. Halasz, A. D. Jackson, R. E. Shrock, M. A. Stephanov and J. J. M. Verbaarschot, Phys. Rev. **D 58**, 096007 (1998).
- [18] O. Scavenius, A. Mocsy, I. N. Mishustin and D. H. Rischke, Phys. Rev. **C 64**, 045202 (2001).
- [19] Y. Hatta and T. Ikeda, Phys. Rev. **D 67**, 014028 (2003).
- [20] A. Barducci, R. Casalbuoni, G. Pettini and L. Ravagli, Phys. Rev. **D 72**, 056002 (2005).
- [21] W. J. Fu, Z. Zhang, and Y. X. Liu, Phys. Rev. **D 77**, 014006 (2008).
- [22] M. A. Stephanov, PoS **LAT2006**, 024 (2006).
- [23] B. Mohanty, Nucl. Phys. **A 830**, 899c (2009); T. Schuster, PoS **CPOD 2009**, 029 (2009); G. Stefanek, PoS **CPOD 2009**, 049 (2009).
- [24] T. Anticic *et al.* (NA49 Collaboration), N. G. Antoniou, F. K. Diakonov, and G. Mavromanolakis, arXiv:0912.4198 [nucl-ex].
- [25] M. M. Aggarwal *et al.* (STAR Collaboration), arXiv:1004.4959 [nucl-ex].
- [26] M. Asakawa, U. W. Heinz, and B. Müller, Phys. Rev. Lett. **85**, 2072 (2000).
- [27] S. Jeon and V. Koch, Phys. Rev. Lett. **85**, 2076 (2000).
- [28] M. A. Stephanov, K. Rajagopal, and E. V. Shuryak, Phys. Rev. Lett. **81**, 4816 (1998).
- [29] M. Stephanov, K. Rajagopal, and E. Shuryak, Phys. Rev. **D 60**, 114028 (1999).
- [30] Y. Hatta and M. A. Stephanov, Phys. Rev. Lett. **91**, 102003 (2003).
- [31] S. Jeon, and V. Koch, in: *Quark Gluon Plasma*, edited by R. C. Hwa, X. N. Wang (World Scientific Publishing, Singapore, 2004), Vol. 3, p.430.

- [32] M. A. Stephanov, Phys. Rev. Lett. **102**, 032301 (2009).
- [33] M. Asakawa, S. Ejiri, and M. Kitazawa, Phys. Rev. Lett. **103**, 262301 (2009).
- [34] M. A. Stephanov, Phys. Rev. **D 81**, 054012 (2010).
- [35] C. Athanasiou, K. Rajagopal, and M. Stephanov, arXiv:1006.4636 [hep-ph].
- [36] A. Bhattacharyya, P. Deb, A. Lahiri, and R. Ray, arXiv:1008.0768 [hep-ph].
- [37] W. J. Fu, Y. X. Liu, and Y. L. Wu, Phys. Rev. **D 81**, 014028 (2010).
- [38] M. Cheng *et al.*, Phys. Rev. **D 79**, 074505 (2009).
- [39] P. N. Meisinger, and M. C. Ogilvie, Phys. Lett. **B 379**, 163 (1996); P. N. Meisinger, T. R. Miller, and M. C. Ogilvie, Phys. Rev. **D 65**, 034009 (2002).
- [40] R. D. Pisarski, Phys. Rev. **D 62**, 111501 (2000); A. Dumitru and R. D. Pisarski, Phys. Lett. **B 504**, 282 (2001); Phys. Lett. **B 525**, 95 (2002); Phys. Rev. **D 66**, 096003 (2002).
- [41] K. Fukushima, Phys. Lett. **B 591**, 277 (2004).
- [42] C. Ratti, M. A. Thaler, and W. Weise, Phys. Rev. **D 73**, 014019 (2006).
- [43] S. Rößner, C. Ratti, and W. Weise, Phys. Rev. **D 75**, 034007 (2007).
- [44] M. Ciminale, R. Gatto, N. D. Ippolito, G. Nardulli, and M. Ruggieri, Phys. Rev. **D 77**, 054023 (2008).
- [45] Z. Zhang, and Y. X. Liu, Phys. Rev. **C 75**, 064910 (2007).
- [46] W. J. Fu, and Y. X. Liu, Phys. Rev. **D 79**, 074011 (2009).
- [47] S. K. Ghosh, T. K. Mukherjee, M. G. Mustafa, and R. Ray, Phys. Rev. **D 73**, 114007 (2006); S. Mukherjee, M. G. Mustafa, and R. Ray, Phys. Rev. **D 75**, 094015 (2007)
- [48] P. Rehberg, S. P. Klevansky, and J. Hüfner, Phys. Rev. **C 53**, 410 (1996).